WILEY

ENABLING DISCOVERY | POWERING EDUCATION | SHAPING WORKFORCES

Epilepsy Knowledge Hub



Access the latest ILAE Guidelines webinars on demand

The Epilepsy Knowledge Hub is intended to provide health care professionals with the latest research and tools to aid in the diagnosis, classification, and subsequent treatment for patients with epilepsy syndromes at various ages.

This resource has been created in coordination with Epilepsia, a peer-reviewed journal published by Wiley on behalf of the International League Against Epilepsy (ILAE). Previous webinars are available on-demand on this site for CME credits.

Visit now

Access the hub for free access to:

Videos

Infographics

Articles

Access now

This educational resource has been supported by Zogenix International Limited, now a part of UCB.
Zogenix International Limited has had no influence over the content or selection of the Editorial Panel.

Oakstone CME

Jointly Provided by Oakstone Publishing and John Wiley and Sons Limited
This activity was planned and implemented in accordance with the accreditation requirements and policies of the Accreditation Council for Continuing Medical Education (ACCME) through the joint providership of Oakstone Publishing and John Wiley and Sons Limited, Oakstone Publishing is accredited by the ACCME to provide continuing medical education for physicians.

Oakstone Publishing designates this recording activity for a maximum of 1.0 AMA PRA Category 1 Credits™. Physicians should claim only the credit commensurate with the extent of their participation in the activity.

Check for updates

Received: 31 July 2019 | Revised: 3 February 2020 | Accepted: 3 February 2020

DOI: 10.1111/epi.16456

FULL-LENGTH ORIGINAL RESEARCH

Epilepsia®

New insights into the early mechanisms of epileptogenesis in a zebrafish model of Dravet syndrome

Ettore Tiraboschi[1] | Silvia Martina[2] | Wietske van der Ent[1] | Kamil Grzyb[2] | Kinga Gawel[1,3] | Maria Lorena Cordero-Maldonado[2] | Suresh Kumar Poovathingal[2] | Sarah Heintz[1] | Somisetty Venkata Satheesh[4] | Jarle Brattespe[5] | Ju Xu[6] | Maximiliano Suster[7] | Alexander Skupin[2] | Camila V. Esguerra[1,8]

[1]Chemical Neuroscience Group, Center for Molecular Medicine Norway, University of Oslo, Oslo, Norway

[2]Integrative Cell Signaling Group, Luxembourg Center for Systems Biomedicine, University of Luxembourg, Esch-sur-Alzette, Luxembourg

[3]Department of Experimental and Clinical Pharmacology, Medical University of Lublin, Lublin, Poland

[4]Molecular Toxicology Group, Institute of Basic Medical Sciences, University of Oslo, Oslo, Norway

[5]Department of Biological Sciences, University of Bergen, Bergen, Norway

[6]Department of Biomedicine, University of Bergen, Bergen, Norway

[7]allmyhomes, Berlin, Germany

[8]Department of Pharmacy, University of Oslo, Oslo, Norway

Correspondence
Camila V. Esguerra, Chemical Neuroscience Group, Center for Molecular Medicine Norway, University of Oslo, Gaustadalléen 21, Forskningsparken 0349 Oslo, Norway.
Email: c.v.esguerra@ncmm.uio.no

Present address
Suresh Kumar Poovathingal, Single Cell Analytics & Microfluidics Core, Vlaams Instituut voor Biotechnologie (VIB)-Katholieke Universiteit (KU) Leuven

Abstract

Objective: To pinpoint the earliest cellular defects underlying seizure onset (epileptogenic period) during perinatal brain development in a new zebrafish model of Dravet syndrome (DS) and to investigate potential disease-modifying activity of the $5HT_2$ receptor agonist fenfluramine.

Methods: We used CRISPR/Cas9 mutagenesis to introduce a missense mutation, designed to perturb ion transport function in all channel isoforms, into *scn1lab*, the zebrafish orthologue of *SCN1A* (encoding voltage-gated sodium channel alpha subunit 1). We performed behavioral analysis and electroencephalographic recordings to measure convulsions and epileptiform discharges, followed by single-cell RNA-Seq, morphometric analysis of transgenic reporter-labeled γ-aminobutyric acidergic (GABAergic) neurons, and pharmacological profiling of mutant larvae.

Results: Homozygous mutant (*scn1lab*$^{mut/mut}$) larvae displayed spontaneous seizures with interictal, preictal, and ictal discharges (mean = 7.5 per 20-minute recording; $P < .0001$; one-way analysis of variance). Drop-Seq analysis revealed a 2:1 shift in the ratio of glutamatergic to GABAergic neurons in *scn1lab*$^{mut/mut}$ larval brains versus wild type (WT), with dynamic changes in neuronal, glial, and progenitor cell populations. To explore disease pathophysiology further, we quantified dendritic arborization in GABAergic neurons and observed a 40% reduction in arbor number compared to WT ($P < .001$; n = 15 mutant, n = 16 WT). We postulate that the significant reduction in inhibitory arbors causes an inhibitory to excitatory neurotransmitter imbalance that contributes to seizures and enhanced electrical brain activity in *scn1lab*$^{mut/mut}$ larvae (high-frequency range), with subsequent GABAergic neuronal loss and astrogliosis. Chronic fenfluramine administration completely restored dendritic arbor numbers to normal in *scn1lab*$^{mut/mut}$ larvae, whereas similar treatment with the benzodiazepine diazepam attenuated seizures, but was ineffective in restoring neuronal

Silvia Martina and Wietske van der Ent contributed equally to this work.

This is an open access article under the terms of the Creative Commons Attribution-NonCommercial License, which permits use, distribution and reproduction in any medium, provided the original work is properly cited and is not used for commercial purposes.
© 2020 The Authors. *Epilepsia* published by Wiley Periodicals, Inc. on behalf of International League Against Epilepsy.

15281167, 2020, 3, Downloaded from https://onlinelibrary.wiley.com/doi/10.1111/epi.16456 by Ku Leuven, Wiley Online Library on [31/10/2022]. See the Terms and Conditions (https://onlinelibrary.wiley.com/terms-and-conditions) on Wiley Online Library for rules of use; OA articles are governed by the applicable Creative Commons License

Center for Brain and Disease Research, Leuven, Belgium

Funding information
Centre for Molecular Medicine Norway (NCMM) Start up grant; National Research Fund of Luxembourg, Grant/Award Number: C14/BM/7975668/CaSCAD and INTER/DFG/17/11583046 MechEPI (Mechanisms of Epileptogenesis)

cytoarchitecture. BrdU labeling revealed cell overproliferation in *scn1lab*$^{mut/mut}$ larval brains that were rescued by fenfluramine but not diazepam.

Significance: Our findings provide novel insights into early mechanisms of DS pathogenesis, describe dynamic cell population changes in the *scn1lab*$^{mut/mut}$ brain, and present first-time evidence for potential disease modification by fenfluramine.

KEYWORDS
Dravet syndrome, epileptogenesis, fenfluramine, sodium channel, zebrafish

1 | INTRODUCTION

Dravet syndrome (DS) is a severe, intractable, pediatric epileptic encephalopathy.[1] Approximately 70%-80% of patients carry de novo mutations in *SCN1A*, which encodes the voltage-gated sodium channel α1 subunit ($Na_v1.1$).[2] Gene variants for *SCN2A, SCN8A, GABRA1,* or *STXBP1* have also been implicated in DS-like epileptic encephalopathies, making DS a heterologous disease, with high phenotypic variability among patients.[3,4] Seizure onset is typically provoked by fever, usually within the first year of life.[1] Patients exhibit prolonged, frequent, and diverse types of seizures, from febrile or afebrile, to generalized myoclonic and/or absence seizures[5] that are refractory to current antiseizure drugs.

Human and mouse $Na_v1.1$ is predominantly expressed in parvalbumin-positive γ-aminobutyric acid (GABA) interneurons,[6] in brain structures playing a critical role in seizure generation and spread,[7,8] such as the hippocampus or cortex.[9,10] $Na_v1.1$ haploinsufficiency impairs Na^+ currents and action potential firing of GABAergic interneurons, leading to an elevated excitation/inhibition ratio in forebrain structures.[6] Moreover, functional and structural dentate gyrus deficits in the hippocampal network parallel spontaneous seizure onset. In particular, dentate gyrus granule cells exhibited reduced dendritic arborization and increased spine density.[11]

In addition to stiripentol and cannabidiol, now approved by the US Food and Drug Administration as add-on therapy for DS, fenfluramine (FEN) has emerged as a promising therapeutic candidate.[12,13] FEN, an amphetaminelike drug initially introduced into the market as an appetite suppressant, acts as an serotonin (5-hydroxytryptamine [5-HT]) receptor type 2A, 2B, and 2C agonist and a strong inducer of 5-HT release. Recently, FEN was proposed to exert antiseizure activity through allosteric modulation of the sigma-1 receptor.[14] An open-label clinical trial using a clinically confirmed cohort of DS patients indicated that seven of 10 patients taking FEN were seizure-free for >1 year (mean = 6 years[15]). Results from phase 3 clinical trials (FEN hydrochloride; Fintepla, ZX008) showed 64% seizure reduction in children taking 0.8 mg/kg/d,[15] which corroborates the report by Zhang et al,[16] who demonstrated FEN efficacy in decreasing mean duration and frequency of epileptiform discharges in a zebrafish *scn1a* knockdown model. Due to concerns associated with FEN and its potential to induce cardiac valve disease and/or pulmonary hypertension,[17] it was withdrawn from the market in 1997. However, the latest retrospective study indicated that long-term treatment with FEN (27 years) did not increase risk of cardiac valvulopathy or pulmonary hypertension.[18]

Key Points

- Zebrafish *scn1lab*$^{mut/mut}$ larvae display dynamic neuronal and glial cell population changes, including GABAergic neuronal loss and astrogliosis
- *scn1lab*$^{mut/mut}$ larvae display strongly reduced dendritic arborization of GABAergic neurons and cell hyperproliferation
- Chronic fenfluramine treatment rescued the observed arborization and cell hyperproliferation defects, whereas diazepam treatment did not

Zebrafish are now a recognized model of epilepsy, with genetic and chemically induced models able to recapitulate characteristic features of epileptiform activity.[19,20] Here, we introduced an indel mutation into *scn1lab,* the zebrafish orthologue of *SCN1A*. We undertook a comprehensive analysis of *scn1lab*$^{mut/mut}$ larvae to obtain insight into the earliest neurodevelopmental and epileptogenic consequences of *scn1lab* dysfunction. Additionally, due to lack of knowledge about the early chronic effects of FEN usage in DS patients, we aimed to clarify whether and how FEN could counteract neurodevelopmental changes in *scn1lab*$^{mut/mut}$ brains.

2 | MATERIALS AND METHODS

2.1 | Zebrafish husbandry

Wild-type (WT) adult zebrafish (*Danio rerio*; AB strain; ZIRC) were maintained at 28.5°C on a 14-h/10-h light/dark

15281167, 2020, 3, Downloaded from https://onlinelibrary.wiley.com/doi/10.1111/epi.16456 by Ku Leuven, Wiley Online Library on [31/10/2022]. See the Terms and Conditions (https://onlinelibrary.wiley.com/terms-and-conditions) on Wiley Online Library for rules of use; OA articles are governed by the applicable Creative Commons License

cycle under standard aquaculture conditions, and fertilized eggs were collected via natural spawning. Embryos were raised in embryo medium (E3; 1.5 mmol/L HEPES, pH 7.6, 17.4 mmol/L NaCl, 0.21 mmol/L KCl, 0.12 mmol/L $MgSO_4$, and 0.18 mmol/L $Ca[NO_3]_2$), under the same conditions as adults. All experiments were approved by the Norwegian Food Safety Authority experimental animal administration's supervisory and application system (FOTS-18/106800-1).

2.2 | Zebrafish lines

The *scn1lab* (c.439_441delATG;443_445delCGC, p.M147_L149delinsI) line, hereafter *scn1lab*$^{mut/mut}$, was generated using CRISPR/Cas9 mutagenesis. The identified founder carried a 6-nucleotide deletion within exon 4 (gRNA sequence: CTGCGCCTTCATGACGCTCAG, Figure S1A). This deletion produced a double amino acid (aa) deletion (Met, Leu) and a single aa change (Thr->Ile; Figure 1A). The aa sequence changed from FMTLSNP to FISNP and affects the ion transport domain (http://www.ebi.ac.uk/interpro/entry/IPR005821; Figure S1B). Dlx5/6:Gal4-T2A-gfp were generated by coinjecting the iTol2_Dlx5/6:Gal4-T2A-gfp plasmid with transposase mRNA. This plasmid was obtained by cloning the dlx6a-1.4kbdlx5a/dlx6a:GFP sequence into a pminiTol2 vector (Addgene #31829).[21] The sequence was taken from the plasmid pcs-dlx6a-1.4kbdlx5a/dlx6a:GFP (gift, Mark

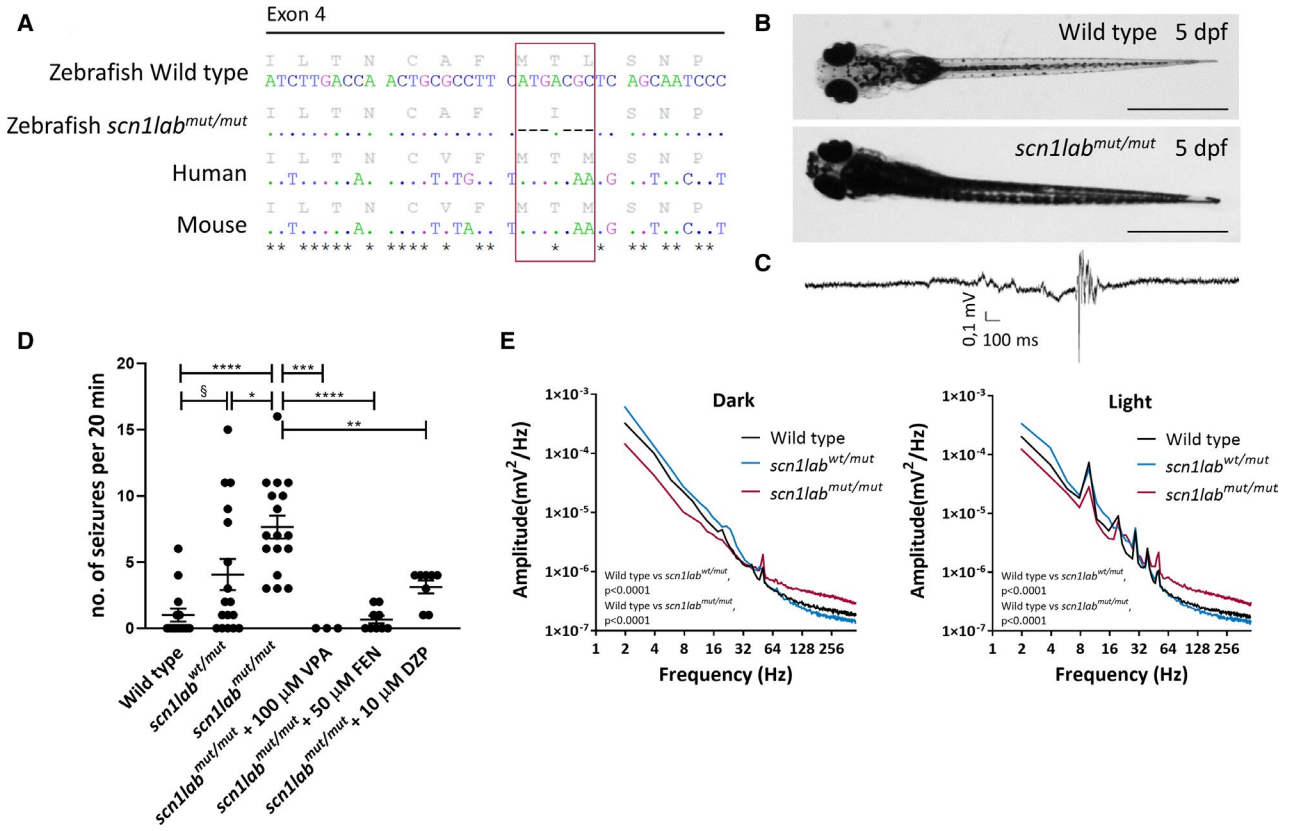


FIGURE 1 Development of *scn1lab*$^{mut/mut}$ zebrafish model by CRISPR/Cas9 technique and its characterization. A, Amino acid and nucleotide sequence of *scn1lab* in zebrafish wild type (WT) and *scn1lab*$^{mut/mut}$, and orthologues in human (*SCN1A*) and mouse (*Scn1a*). Dots indicate identical nucleotides, dashes indicate deletions, and stars indicate identical nucleotides in all four sequences. B, WT and *scn1lab*$^{mut/mut}$ larvae at 5 days postfertilization (dpf). Increased pigmentation is observed in mutants. Scale bars = 1 mm. C, Example of local field potential (LFP) recording obtained from the *scn1lab*$^{mut/mut}$ tectum at 5 dpf, showing a seizure event with preictal and ictal phase. D, *scn1lab*$^{mut/mut}$ larvae at 5 dpf show an increased number of seizures over a 20-minute period compared to WT larvae or *scn1lab*$^{wt/mut}$ siblings. A low number of seizures were observed in WT larvae, likely caused by needle insertion into the optic tectum. *scn1lab*$^{wt/mut}$ displayed a larger number of seizures on average than WT larvae, but more interindividual variability was observed, with some larvae displaying no seizures, whereas others were affected to the same extent as homozygous larvae. No significant difference in the number of seizures was observed between WT larvae and *scn1lab*$^{mut/mut}$ larvae treated with valproic acid (VPA), fenfluramine (FEN), or diazepam (DZP), indicating efficacy of these drugs in reducing the number of seizures to background levels. Significance was calculated using one-way analysis of variance with Tukey post hoc test (*$P < .05$, **$P < .01$, ***$P < .001$, ****$P < .0001$) or unpaired, two-tailed *t* test (§$P < .05$). E, Power spectrum analyses of LFP recordings performed under dark conditions, or under a 10-Hz flashing light stimulus. The energy profile of *scn1lab*$^{mut/mut}$ larvae differs significantly from WT and *scn1lab*$^{wt/mut}$ siblings in both conditions. A Kolmogorov-Smirnov test was used to calculate significance

15281167, 2020, 3, Downloaded from https://onlinelibrary.wiley.com/doi/10.1111/epi.16456 by Ku Leuven, Wiley Online Library on [31/10/2022]. See the Terms and Conditions (https://onlinelibrary.wiley.com/terms-and-conditions) on Wiley Online Library for rules of use; OA articles are governed by the applicable Creative Commons License

Ekker). Subsequently, a polymerase chain reaction (PCR) fragment containing Gal4-T2A was inserted in-frame with green fluorescent protein by blunt end ligation into the final plasmid.

2.3 | Locomotor tracking

Locomotor activity was assessed as previously described,[20] with modifications. Four- and 7-days postfertilization (dpf) larvae were placed in 48-well plates (one larva/well) containing 300 μL medium and habituated for 15 minutes to the apparatus (ZebraBox, Viewpoint). Larvae were tracked for 60 minutes in light/dark phase, with 5-minute integration intervals. Measurements were performed at the same daytime period. Distance covered by each larva was recorded in millimeters. Two independent experiments were performed (n = 44-48/group/phase), and the data were pooled.

2.4 | Local field potential recordings

Recordings were obtained from tecta at 4 and 5 dpf as described.[20] Seizure detection was performed through visual inspection and automated using a custom-written R script to minimize bias and artifacts due to muscle contractions. Recorded frequencies were categorized into three bands (1-100, 100-250, and 250-500 Hz). If amplitude exceeded 3× background, the event was considered a seizure. This method was based on high-frequency oscillations (>100 Hz) as a reported marker of epileptic activity.[22] Power spectrum was analyzed using Clampfit 10.2 software (Molecular Devices). Four-minute-long recordings were used for computing the power spectrum from larvae at 5 dpf, and each condition was averaged per group. Light stimuli were generated with a custom-made device comprising an Arduino board sending a 10-Hz sinusoidal wave to a transistor, which in turn powered a 2-W light-emitting diode emitting white light. Light was delivered via optic fiber to the recording stage.

2.5 | Real-time quantitative PCR

Heads of 6-dpf anesthetized larvae were collected in pools of 10 for RNA extraction. RNA was purified using TRIzol, and cDNA was synthesized using the SuperScript IV First-Strand Synthesis System (Invitrogen). cDNA was amplified using PowerUp SYBR Green Master Mix (Applied Biosystems) according to the manufacturer's instructions. Relative enrichment was computed according to the $2^{-\Delta\Delta t}$ method.[23] Expression levels were normalized against β-actin. Primer sequences were actb2_f_5'TTCTCTTAAGTCGACAACCCCC3', actb2_r_5'ACAATACCGTGCTCGATGGG3'; elavl3_f_5'ATCAACACGCTCAACGGTCT3', elavl3_r_5'TTACCAGGATGCGTGAGGTG3'; gad67_f_5'TGTGTCCGATGGCTTGAGTC3', gad67_r_5'CACACGGAGGATGGTTCACA3'; and vglut1_f_5'CGGCTCATTCTTCTGGGGTT3', vglut1_r_5'GACCATGATCACACACCCGT3'.

2.6 | Single-cell transcriptomics

Brain dissections, cell dissociations, encapsulation, and generation of microfluidic Drop-Seq chips were performed in accordance with the Drop-Seq protocol[24] as described (detailed in Supplementary Methods in Data S1).

2.7 | Bioinformatics

Sequencing data were processed by the Drop-Seq bioinformatics pipeline (v1.13), and reads were mapped against genome version GRCz11.92, resulting in corresponding digital expression matrices. Data analysis was performed by Monocle (v2.4.0) in R (v3.4.4) following the standard workflow for quality control, dimension reduction, and differential expression analysis (see Supplementary Methods in Data S1).

2.8 | Imaging and quantification of arbors

To visualize GABAergic neurons, *scn1lab*$^{wt/mut}$ fish were crossed with Dlx5/6:Gal4-T2A-gfp/UAS:nfsb-mCherry reporter line. Adults were then in-crossed for generating *scn1lab*$^{mut/mut}$. For controls, Dlx5/6:Gal4-T2A-gfp/UAS:nfsb-mCherry fish were crossed with WT. Larvae were treated from 1 dpf with 0.003% phenylthiourea, to prevent pigmentation. FEN (50 μmol/L) or diazepam (DZP; 10 μmol/L) was added to E3 medium at 3 dpf and replaced daily until 6 dpf. Larvae were anesthetized in 0.001% tricaine (Sigma), fixed for 3 hours at room temperature with 4% paraformaldehyde, mounted on glass slides, and imaged using confocal microscopy. A dorsal z-stack of the optic tectum was collected using a ×40 lens and a z-resolution of 0.44 μm. For Sholl analysis,[25,26] images were filtered using the 3D-Median filter in ImageJ. A z-projection of the tectum was generated, and the resulting image was converted to a thresholded binary image. The extent of arborization was quantified using Sholl analysis (plug-in; http://imagej.net/Sholl_Analysis). The number of intersections was normalized against the number of neurons quantified in the imaged area, and this value was used for statistical analysis.

15281167, 2020, 3, Downloaded from https://onlinelibrary.wiley.com/doi/10.1111/epi.16456 by Ku Leuven, Wiley Online Library on [31/10/2022]. See the Terms and Conditions (https://onlinelibrary.wiley.com/terms-and-conditions) on Wiley Online Library for rules of use; OA articles are governed by the applicable Creative Commons License

2.9 | BrdU immunohistochemistry

BrdU labeling was performed as described in Supplementary Methods (Data S1).

2.10 | Statistical analysis

Data were analyzed using GraphPad Prism 7.05. For multiple comparisons, one-way analysis of variance followed by Tukey or Sidak post hoc test was used. Students unpaired *t* test or Kolmogorov-Smirnov test was performed if necessary. For single-cell RNA-Seq (scRNA-Seq) analysis, Bonferroni compensation for multiple testing was used when applicable.

3 | RESULTS

3.1 | *scn1lab*$^{mut/mut}$ larvae recapitulate features of DS

We generated a zebrafish line, using CRISPR/Cas9 mutagenesis, carrying a double aa deletion and single aa substitution in the first ion transport domain of *scn1lab* (Figure S1). Morphologically, *scn1lab*$^{mut/mut}$ larvae phenocopied previously described zebrafish *scn1lab* loss-of-function models, displaying hyperpigmentation from 4 dpf and uninflated swim bladders.[16,27] At 5 dpf, a "kink" posterior to the trunk became evident and larvae struggled to maintain an upright posture (Figure 1B). Homozygotes survive until 14 dpf, whereas heterozygotes breed well and remain healthy up to 18 months. We assessed locomotor activity[16,19,20] at 4 and 7 dpf. *scn1lab*$^{mut/mut}$ larvae were more active and traveled greater distances in light phase compared to WT. However, whereas WT siblings tested in dark phase increased locomotor activity, *scn1lab*$^{mut/mut}$ larvae displayed minimal increase in movement in dark conditions (Figure S2). Touch response in 5-dpf *scn1lab*$^{mut/mut}$ larvae was comparable to WT, with delayed touch response in two of 24 mutant larvae versus one of 24 WT larvae (data not shown). Tectal field recordings indicated that both *scn1lab*$^{mut/mut}$ and *scn1lab*$^{wt/mut}$ larvae displayed seizures starting from 4 dpf (Figure 1D, Figure S3). Five-days-postfertilization *scn1lab*$^{mut/mut}$ larvae (n = 17) displayed spontaneous electrographic discharges with high amplitude and duration (Figure 1C,D), which were inhibited by acute administration of 100 µmol/L valproic acid (VPA; $P < .001$; n = 3), 50 µmol/L FEN ($P < .0001$; n = 9), or 10 µmol/L DZP ($P < .01$; n = 8; Figure 1D). We then performed electroencephalography (EEG) with alternating periods of stimulus deprivation or photostimulation, by recording larvae in the dark or delivering a 10-Hz sine wave flashing light. Spectral EEG analyses revealed that *scn1lab*$^{mut/mut}$ larval (n = 11) energy profiles differed significantly from heterozygous (n = 8) and WT counterparts ($P < .0001$; n = 11).

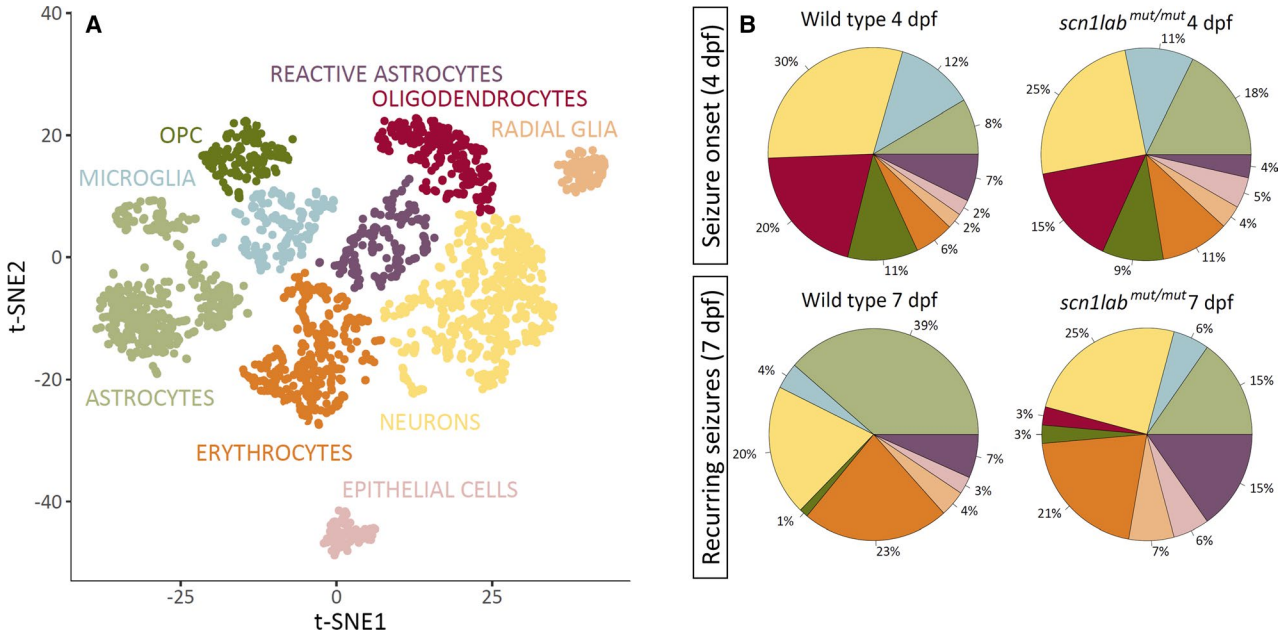


FIGURE 2 Single-cell RNA-Seq data reveals changes in brain composition. A, The 2508 clearly identified cells were clustered and cell identities inferred by cell type-specific scores (Figure S4) based on marker genes (Table S1). Interestingly, distinct astrocytic clusters were identified that indicate maturation of cells (Figure S4). OPC, oligodendrocyte progenitor cells. B, The brain composition exhibits an increase in radial glia at 7 days postfertilization (dpf) for both cell lines and a doubled percentage of reactive astrocytes in *scn1lab*$^{mut/mut}$ cells. The strongly reduced number of oligodendrocytes at 7 dpf probably results from damage during cell isolation and corresponding leakage of mRNAs (Figure S5). Cell clusters presented here are from pooled larval brains derived from wild type or homozygotes. tSNE, T-distributed Stochastic Neighbor Embedding

15281167, 2020, 3, Downloaded from https://onlinelibrary.wiley.com/doi/10.1111/epi.16456 by Ku Leuven, Wiley Online Library on [31/10/2022]. See the Terms and Conditions (https://onlinelibrary.wiley.com/terms-and-conditions) on Wiley Online Library for rules of use; OA articles are governed by the applicable Creative Commons License

In particular, energy distribution at high frequencies (>100 Hz) was greater (Figure 1E).

3.2 | Brain composition analysis

We performed scRNA-Seq analysis using our Drop-Seq pipeline (see Supplementary Methods in Data S1). Epithelial cells formed a distinct subpopulation (light red cluster), and neuronal- and glia-related clusters were separated well. Astrocytes formed subclusters, and radial glia exhibited a specialized expression profile leading to a distinct cluster (Figure 2A). Comparison of cell type matching with sample identity (Figure S5) did not indicate a *scn1lab*$^{mut/mut}$-specific neuronal expression profile but reduced astrocytic maturation. Increased vascularization became apparent from the increased number of erythrocytes at 7 dpf (Figure 2B). Oligodendrocyte absence at 7 dpf for both conditions is related to the exclusion of leaking cells, as the majority of these were associated with 7-dpf samples and careful evaluation of the corresponding expression profiles indicated their oligodendrocytic origin by the remaining her4.1 transcripts (Figure S5). The relative decrease in the neuronal subpopulation was also caused by an increase in astrocytes in both lines where, in particular, radial glia appeared to be enriched in *scn1lab*$^{mut/mut}$ larvae.

3.3 | Reduced GABAergic neurons and increased gliosis

We investigated GABAergic and glutamatergic neurons by calculating subtype-specific scores based on relative marker gene expression (Table S1, Figure S6). Glutamatergic scores were similar for *scn1lab*$^{mut/mut}$ and WT, exhibiting an increase from 4 to 7 dpf, where only the increase

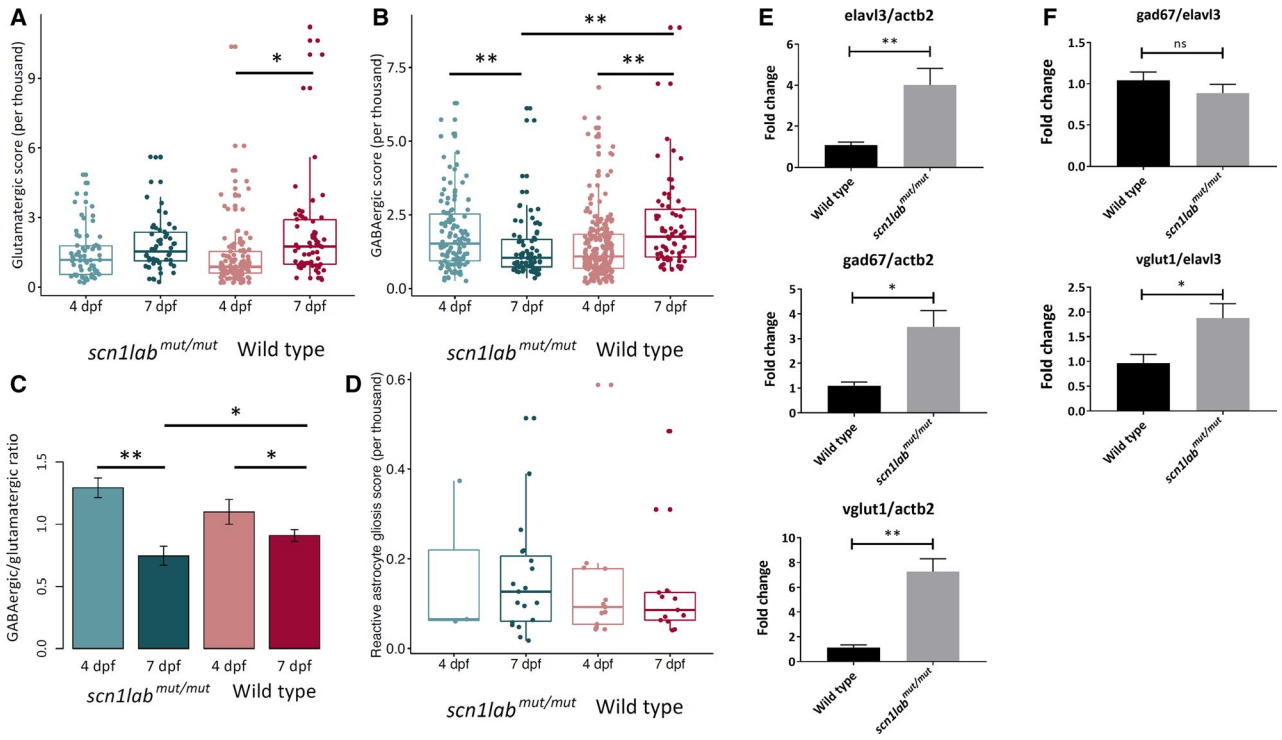


FIGURE 3 Single-cell RNA-Seq data reveal changes in γ-aminobutyric acidergic (GABA) and glutamatergic profiles defined by corresponding marker genes during development and between conditions. A, The glutamatergic score indicates a stronger increase of glutamatergic profiles in wild-type (WT) than in *scn1lab*$^{mut/mut}$ larvae from 4 to 7 days postfertilization (dpf). B, The GABA-related score indicates a significant decrease in neurons of *scn1lab*$^{mut/mut}$ larvae and an increase in WT from 4 to 7 dpf, leading to a significant difference between the conditions. C, Combining these scores to investigate the balance between GABA- and glutamate-related neurons shows a dramatic change in *scn1lab*$^{mut/mut}$ larvae, where the ratio between GABAergic and glutamatergic profiles is reduced by nearly 50% at 7 dpf compared to 4 dpf, whereas in WT only a minor reduction is observed. This results in a significant difference between *scn1lab*$^{mut/mut}$ and WT larvae at 7 dpf and may indicate an underlying mechanism of epileptogenesis. D, The increased number of reactive astrocytes found in *scn1lab*$^{mut/mut}$ do also exhibit an increased gliosis activity defined by corresponding marker genes (Table S1) at 7 dpf, as indicated by differentially expressed gene analysis. E, At 6 dpf, *scn1lab*$^{mut/mut}$ larvae had an increased expression of glutamatergic (*vglut1*), GABAergic (*gad67*), and postmitotic (*elavl3*) neuronal markers compared to WT siblings, as measured by real-time quantitative polymerase chain reaction. F, Upregulation of the excitatory system (as observed by normalization of *vglut1* over *elavl3*), but not the inhibitory system (as observed by normalization of *gad67* over *elavl3*), indicates a shift in the GABA/GLUT population ratios in the brain of *scn1lab*$^{mut/mut}$ larvae. *$P < .05$, **$P < .01$. ns, not significant

15281167, 2020, 3, Downloaded from https://onlinelibrary.wiley.com/doi/10.1111/epi.16456 by Ku Leuven, Wiley Online Library on [31/10/2022]. See the Terms and Conditions (https://onlinelibrary.wiley.com/terms-and-conditions) on Wiley Online Library for rules of use; OA articles are governed by the applicable Creative Commons License

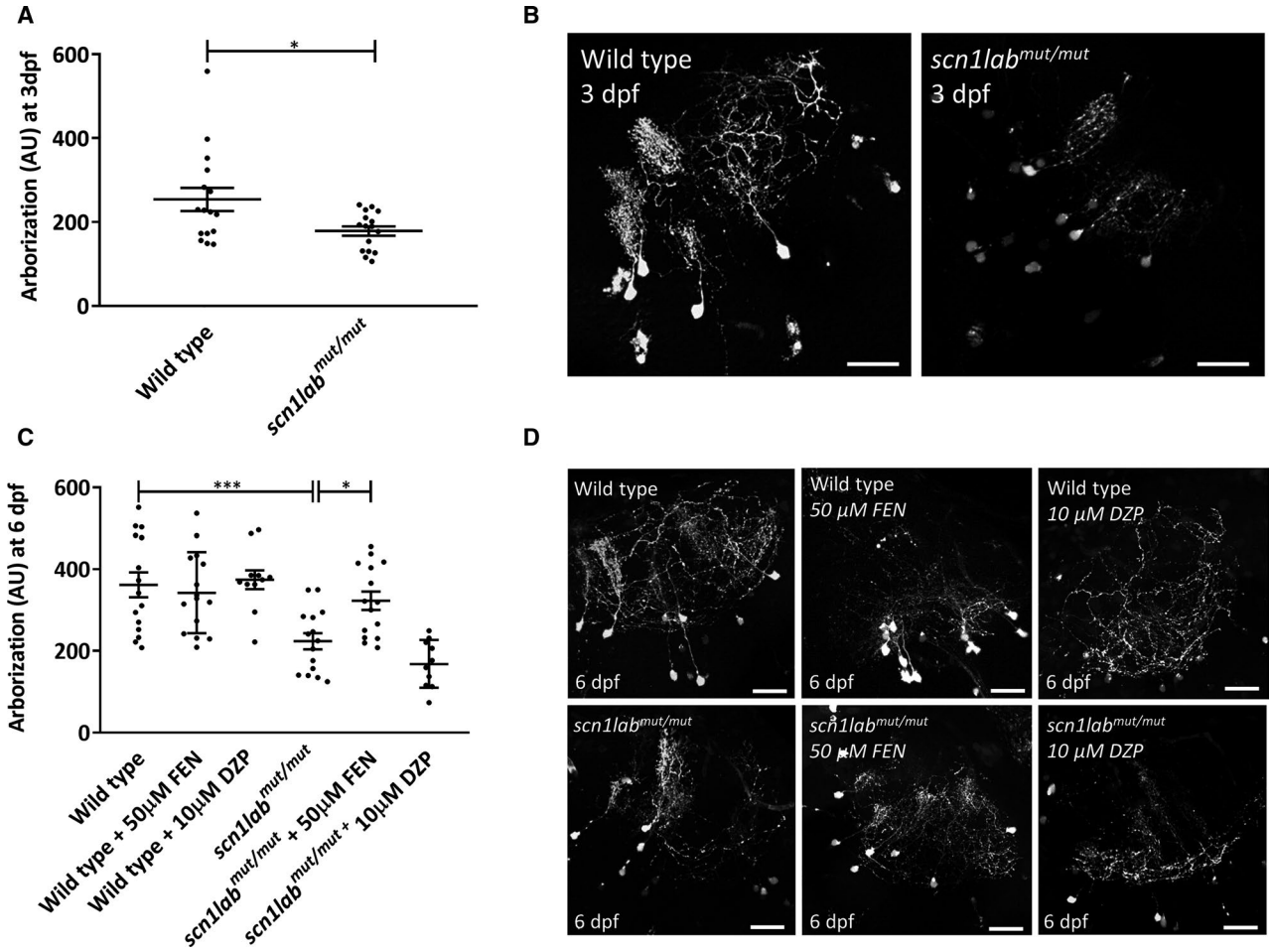


FIGURE 4 Dendritic arborization in *scn1lab*$^{mut/mut}$ larvae. A, *scn1lab*$^{mut/mut}$ larvae show a reduced number of dendritic arbors at 3 days postfertilization (dpf). Significance of differences was calculated using an unpaired, two-tailed *t* test. **P* < .05. B, Representative images of dendritic arbors in the neuropil of wild-type (WT) and *scn1lab*$^{mut/mut}$ larvae at 3 dpf. Scale bars = 25 µm. C, Reduction in dendritic arborization in *scn1lab*$^{mut/mut}$ larvae observed at 6 dpf can be rescued by the addition of 50 µmol/L of fenfluramine (FEN), but not 10 µmol/L of diazepam (DZP), from 3 dpf until 6 dpf. Significance of differences was calculated using one-way analysis of variance with Sidak post hoc test. **P* < .05, ****P* < .001. D, Representative images of dendritic arbors in the neuropil of WT and *scn1lab*$^{mut/mut}$ larvae at 6 dpf, with or without prior incubation in 50 µmol/L of FEN or 10 µM of DZP from 3 dpf onward. Scale bars = 25 µm

in WT was statistically significant (Figure 3A). In contrast, GABAergic scores revealed significant differences during development and between WT and mutant. Whereas the GABAergic score of *scn1lab*$^{mut/mut}$ larvae showed a significant reduction from 4 to 7 dpf, WT larvae exhibited a significant increase in GABAergic marker levels at 7 dpf (Figure 3B). Consequently, *scn1lab*$^{mut/mut}$ larvae had significantly reduced GABAergic marker expression at 7 dpf compared to WT. The similar expression of glutamatergic markers and the significant differences in the GABAergic score led to a distinct shift in the ratio between GABAergic and glutamatergic scores (Figure 3C). Whereas the ratio was slightly reduced in WT (10%), *scn1lab*$^{mut/mut}$ larvae exhibited a reduction of 43% at 7 dpf and a significant decrease (19%) in WT at 7 dpf.

To investigate the increased number of reactive astrocytes in *scn1lab*$^{mut/mut}$ larvae at 7 dpf further, we performed differentially expressed gene analysis and found an enrichment of gliosis-related genes. We calculated a gliosis score based on marker genes (Table S1) and found a trend for higher gliosis activity in reactive astrocytes of *scn1lab*$^{mut/mut}$ larvae (Figure 3D, Figure S6). To test whether the decrease in GABAergic cells correlated with a change in neuronal morphology at the expression level, we targeted axonogenesis-related genes (Table S1) in the scRNA-Seq data. Although we could not find a significant effect on branching expression levels, we observed a trend toward downregulation of neuronal branching genes in the mutant (18%), whereas WT larvae exhibited a nonsignificant reduction of 6% (Figure S7).

To confirm that the distinct EEG energy profile of *scn1lab*$^{mut/mut}$ is caused by increased synaptic activity due to reduced inhibitory tone, we used real-time quantitative PCR to quantify glutamatergic (*vglut1*), GABAergic

15281167, 2020, 3, Downloaded from https://onlinelibrary.wiley.com/doi/10.1111/epi.16456 by Ku Leuven, Wiley Online Library on [31/10/2022]. See the Terms and Conditions (https://onlinelibrary.wiley.com/terms-and-conditions) on Wiley Online Library for rules of use; OA articles are governed by the applicable Creative Commons License

(*gad67*), and postmitotic (*elavl3*) neuronal markers in larval brains. Homozygous *scn1lab*$^{mut/mut}$ had increased expression of all markers compared to WT ($P < .001$, *elavl3/actb2* and *vglut1/actb2*; $P < .05$, *gad67/actb2*; n = 7; Figure 3E). However, normalization of *vglut1* expression against *elavl3* indicated upregulation of excitatory markers ($P < .05$), whereas normalization of *gad67* expression against *elavl3* showed no differences between *scn1lab*$^{mut/mut}$ and WT ($P > .05$; Figure 3F).

3.4 | Neuronal defects restored by FEN

The amplitude difference in the power spectrum observed between *scn1lab*$^{mut/mut}$ and WT indicated possible alteration in optic tectum cytoarchitecture. We therefore quantified dendritic arborization in GABAergic neurons, as reduced branching would explain reduced inhibitory tone. Sholl analysis revealed a 30% decrease ($P < .05$; n = 16) in dendritic arborization of GABAergic tectal neurons of 3 dpf *scn1lab*$^{mut/mut}$ larvae compared to WT (n = 16; Figure 4A,B). By 6 dpf, dendritic arbors were reduced by 40% ($P < .001$; n = 15; Figure 4C,D). As acute FEN treatment effectively suppressed seizures in previously described zebrafish DS models,[16,28] we tested whether chronic FEN administration might affect dendritic morphology. We administered 50 µM FEN chronically for 3 consecutive days, starting at 3 dpf, prior to seizure onset. Chronic treatment of *scn1lab*$^{mut/mut}$ larvae with FEN significantly ($P < .05$; n = 15) abrogated the reduction in dendritic arborization, whereas chronic treatment of WT did not induce any changes ($P > .05$; n = 15; Figure 4C,D). Chronic treatment of *scn1lab*$^{mut/mut}$ larvae with DZP attenuated seizures but showed no amelioration of reduced arborization (Figure 4C,D).

We also evaluated changes in cell proliferation through BrdU labeling in *scn1lab*$^{mut/mut}$ brains. We observed an increase ($P < .01$; n = 8) in BrdU-positive cells, compared to WT at 6 dpf (n = 16; Figure 5). To test whether FEN might also regulate cell proliferation, we exposed *scn1lab*$^{mut/mut}$ larvae to FEN as described above. FEN restored ($P < .05$; n = 9) the number of BrdU-positive tectal cells to untreated WT baseline. FEN treatment of WT also increased ($P < .0001$; n = 7) BrdU-positive cells when compared to untreated WT controls (Figure 5).

4 | DISCUSSION

4.1 | New zebrafish mutant to study DS epileptogenesis

The *scn1lab* mutant described here replicates classic features of DS and recapitulates both previously described phenotypes for other zebrafish *scn1lab* loss-of-function models and *Scn1a* mouse mutants.[4,6,27,28] *didy* homozygotes, however,

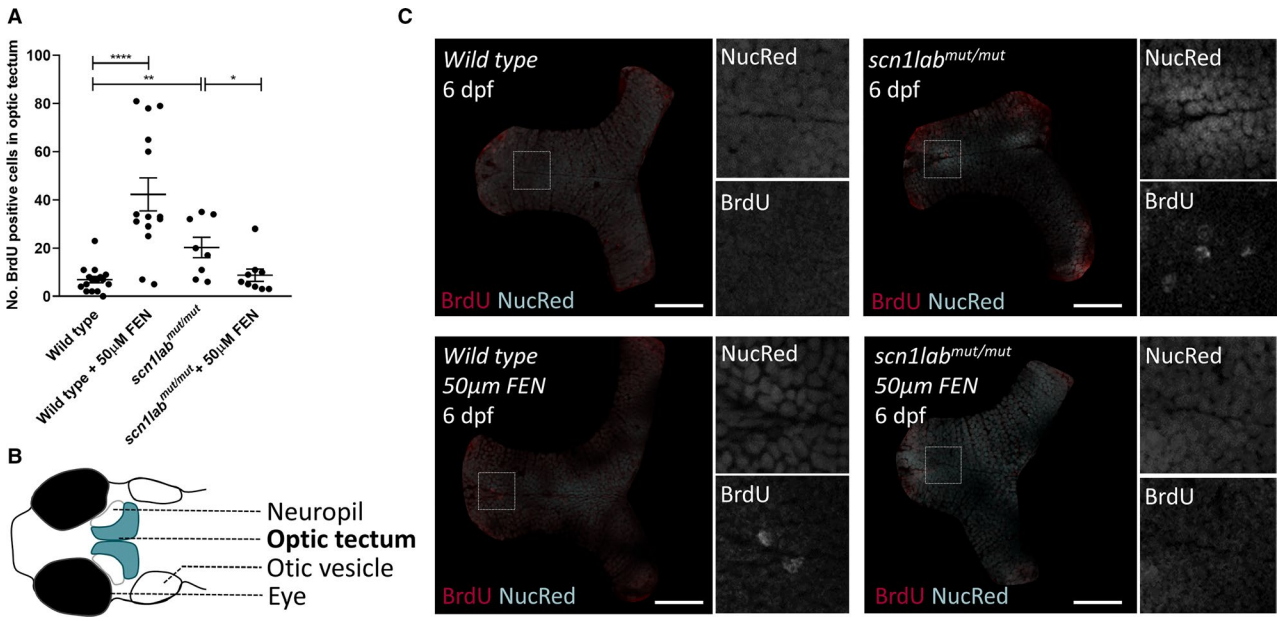


FIGURE 5 Proliferation of cells in the optic tectum of *scn1lab*$^{mut/mut}$ larvae. A, At 6 days postfertilization (dpf), *scn1lab*$^{mut/mut}$ larvae showed an increased number of proliferating cells in the optic tectum, as measured by BrdU-positive cells in 30-µm-thick optical sections. Incubation of larvae in 50 µmol/L of fenfluramine (FEN) from 3 dpf onward resulted in an increased number of BrdU-positive cells in wild-type (WT) larvae at 6 dpf, while reducing the number to untreated WT levels in the *scn1lab*$^{mut/mut}$ larvae. Statistical significance was calculated using multiple unpaired, two-tailed *t* tests. *$P < .05$, **$P < .01$, ****$P < .0001$. B, Cartoon representation of the head of a 6-dpf larva, indicating the position of the optic tectum where proliferation was measured. C, Representative z-slices of masked optic tecta with BrdU staining of WT and *scn1lab*$^{mut/mut}$ larvae at 6 dpf, with or without prior incubation in 50 µmol/L of FEN from 3 dpf onward. Squares indicate the location of the zoomed-in, split-channel images to the right. Scale bars = 50 µm

15281167, 2020, 3, Downloaded from https://onlinelibrary.wiley.com/doi/10.1111/epi.16456 by Ku Leuven, Wiley Online Library on [31/10/2022]. See the Terms and Conditions (https://onlinelibrary.wiley.com/terms-and-conditions) on Wiley Online Library for rules of use; OA articles are governed by the applicable Creative Commons License

survive until 10 dpf,[28] whereas *scn1lab*$^{mut/mut}$ larvae survive until 14 dpf. Moreover, seizures were only reported in *didy* homozygotes, whereas seizures were also observed in *scn1lab*$^{wt/mut}$ heterozygotes, possibly attributable to differences in genetic background or the nature of the mutation (nonsense vs missense).

4.2 | Increased brain excitability

The higher energy distribution observed in *scn1lab*$^{mut/mut}$ brains, both after photostimulus and under dark conditions, indicated that the summation signal of dendritic potentials was excitatory. This is not surprising, given the development of spontaneous seizures, but the finding that this is mostly represented in the high-frequency gamma band was suggestive not only of increased synaptic activity but possibly of decreased inhibitory tone. Neuronal hyperactivity, driven primarily by reduced background inhibition, can be caused by various mechanisms. For example, abnormal gamma-band activity has been observed in schizophrenia patients and related animal disease models as a result of impaired GABAergic neurotransmission, particularly in parvalbumin-expressing neurons.[29] Regarding *SCN1A*-derived disorders, two mechanisms underlying neuronal hyperexcitability have been proposed: impaired interneuron sodium channel activity or increased pyramidal neuron excitability.[30] With regard to the former, studies on mouse *Scn1a* mutants support the hypothesis of disinhibition resulting from decreased $Na_v1.1$ function in interneurons.[9,31]

4.3 | GABAergic neuron loss

There is sufficient evidence that loss of GABAergic neurons is a consistent finding among all models of acquired epilepsy including kindling, status epilepticus, and traumatic brain injury as well as a frequently observed hallmark of temporal lobe epilepsy (TLE).[32–37] Furthermore, selective loss of GABAergic neurons can also give rise to an epileptic state in genetic models. Mice with loss of *Dlx1*, which encodes a transcription factor regulating GABAergic interneuron development, develop epilepsy as a result of a time-dependent reduction in the number of these neurons within the cerebral cortex and hippocampus.[38]

A previous study reported no evident loss of GABAergic neurons in the zebrafish *scn1lab* mutant *didy*.[27] Possible explanations for this discrepancy in cellular phenotype between the models are differences in mutation type and/or the genetic background. Another plausible explanation is that we analyzed GABAergic neuron population dynamics at a later developmental stage (7 dpf instead of 5 dpf as carried out in the *didy* study) and therefore after a longer period of spontaneous recurring seizures. Our data at 4 dpf corroborate with the *didy* study findings of no evident cell loss. Interestingly, our data indicate that there is a slight increase in GABAergic neurons at this earlier time point in the mutant, indicating changes in cell proliferation in the mutant during brain development. Furthermore, we found no difference in glutamatergic marker levels between the conditions but an increase from 4 to 7 dpf. Thus, by 7 dpf, the decrease in the GABAergic neuron signature and the increase in glutamatergic signature indicated a shift in the GABA/GLUT ratio in *scn1lab*$^{mut/mut}$ larvae, providing additional evidence for decreased inhibitory tone.

Importantly, a proportion of GABAergic neurons still remain in mutant larvae, as has been observed in *Scn1a* mouse models, other models of acquired epilepsy, and human TLE. Alterations in the remaining GABAergic neurons of these mammalian models have been proposed as contributors to epileptogenesis. Critical changes resulting in the establishment of an epileptic state include impaired function of remaining GABAergic neurons and morphological changes that eventually lead to aberrant circuitry.[39]

4.4 | Reduced dendritic arborization

The significant reduction in dendritic branching of GABAergic neurons prior to seizure onset in our DS model shows that structural deficits are established well before the epileptic phenotype arises. This indicates that seizures per se are not the primary cause of the observed arborization defects and that the converse may be true; reduced arborization is a possible primary mechanism underlying seizures in DS. Importantly, these defects arose when GABA was still excitatory, that is, prior to the GABA developmental switch, which occurs at 2.5 dpf in zebrafish. The early branching defects in GABAergic neurons are thus likely to be due to the inability of these neurons to propagate action potentials, which in turn impairs strengthening and pruning of synaptic connections. In general, dysfunctional voltage-gated sodium channels would lead to impaired action potentials and current in GABAergic inhibitory neurons,[6,39] lowering inhibitory tone and consequently increasing overall network excitability, which would dramatically alter plasticity, morphology, network dynamics, and functional topology of the neural circuitry. A similar mechanism was proposed for the zebrafish *scn1lab* mutant *didy*, originally described as displaying an abnormal optokinetic response due to its inability to sustain saccade eye movements when presented with a repeating visual stimulus pattern.[40] The authors postulated that depleting *scn1a* channel function in *didy* could potentially reduce channel density, in turn resulting in prolonged stimulation that would eventually deplete the pool of activatable channels and ultimately render neurons unexcitable.

15281167, 2020, 3, Downloaded from https://onlinelibrary.wiley.com/doi/10.1111/epi.16456 by Ku Leuven, Wiley Online Library on [31/10/2022]. See the Terms and Conditions (https://onlinelibrary.wiley.com/terms-and-conditions) on Wiley Online Library for rules of use; OA articles are governed by the applicable Creative Commons License

4.5 | FEN treatment rescues dendritic arborization defects

FEN, a serotonin 5-HT_{2A} and 5-HT_{2C} receptors agonist, is highly effective in diminishing seizures in reported zebrafish DS models. Surprisingly, there are no reports describing effects of chronic or acute FEN treatment in DS rodent models. A recent study that evaluated selective 5-HT_{2C} agonists lorcaserin, CP809101, and FEN in multiple acute rodent seizure models (maximum electroshock seizure [MES], MES threshold, 6-Hz electrical convulsive seizure, pentylenetetrazole, and amygdala kindling), showed that with the exception of FEN-mediated tonic seizure inhibition in the MES rat test, there was no antiseizure effect for all compounds in all other tests.[41] The authors concluded that early developmental genetic models might be more appropriate for study of certain drug leads, indicating a need to consider integrating additional animal models into preclinical drug discovery pipelines.

Chronic treatment with FEN prevents cell overproliferation in *scn1lab*$^{mut/mut}$ larvae. However, in WT larvae it increases cell proliferation. These results corroborate previous findings that showed neurogenesis-stimulating activity of antidepressants in the dentate gyrus.[42] The role of serotonin in regulating interneuron morphology has previously been shown. Inhibition of serotonin synthesis in rat embryos with para-chlorophenylalanine disrupted pyramidal neuron maturation within the somatosensory cortex by reducing dendritic arborization.[43] Benzodiazepines such as DZP and clobazam have been used to treat DS.[18] Our data suggest that FEN activity is specific and not simply due to seizure inhibition, as chronic treatment using DZP did not restore dendritic arbor numbers to normal.

Dendritic arborization defects have also been reported for *Scn1a*$^{E1099X/+}$ and *Scn1b*$^{C121W/+}$ mice.[11,44] *Scn1a*$^{E1099X/+}$ mice display progressively reduced dendritic arborization and excessive spines in GABAergic hippocampal dentate gyrus neurons, whereas *Scn1b*$^{C121W/+}$ mice exhibit reduced arborization in subicular pyramidal neurons. These morphological abnormalities, however, were analyzed coincident with (ie, not prior to) developmental spontaneous seizure onset. It is therefore unclear whether arborization defects in these models were a key trigger for epileptogenesis or a consequence thereof. Clearly, further investigation is warranted to determine the exact role of dendritic arborization in DS pathogenesis. Such studies would require dendrite morphology analysis in our DS model at later developmental stages, to allow for sufficient drug washout after chronic FEN or DZP administration (to rule out acute seizure inhibition from residual drug), ideally resulting in significant seizure reduction or freedom in FEN-rescued but not DZP-treated larvae.

4.6 | Gliosis

Radial glial cells are more abundant in *scn1lab* mutants compared to WT, with a doubling of reactive astrocytes in the mutant relative to WT, indicating a trend toward increased gliosis. Reactive astrocytes increase in number as a consequence of epileptic events but are also suggested to play a functional role in the causation of seizures, for instance, after brain trauma.[45] Our scRNA-Seq results are in line with a previous study that compared RNA-Seq data obtained from *Scn1a*$^{\pm}$ mice on two different strains. Half of differentially expressed genes shared between the two models were associated with astrogliosis, including genes upregulated in response to human and rodent seizures or traumatic brain injury.[46]

As mentioned, heterozygous *scn1lab* mutant larvae described in this study also display frequent seizures yet are fertile and survive to adulthood. This could prove useful for analyzing *Scn1a* dysfunction during later stages of epileptogenesis for studying comorbid features and for testing disease-modifying activity of drugs in the context of a mature brain. The astrogliosis phenotype is also worth characterizing further. Notably, a study that performed electrophysiological recordings on acute brain slices from *Scn1a*$^{\pm}$ mice found that, at later developmental stages, parvalbumin-positive fast-spiking basket cell interneuron excitability normalized. The results of this study implied that impairing action potential generation by parvalbumin-positive fast-spiking basket cell interneurons contribute to the initial epilepsy phenotype but may not be the sole mechanism that drives later, chronic epilepsy in DS.[47] It is equally important, however, to consider that the variable severity and expressivity of the murine *Scn1a*$^{\pm}$ epilepsy phenotype is highly strain dependent.[48,49] Therefore, it will be interesting to explore whether stabilization of interneuron activity can be recapitulated in the zebrafish *scn1lab*$^{wt/mut}$.

This study describes a new zebrafish *scn1a* channelopathy model that recapitulates many aspects of DS and may prove useful in identifying other disease mechanisms such as the role of neuron-glia interaction and glutamatergic neurons in the process of epileptogenesis or the development of other associated comorbidities. These data illustrate the utility of zebrafish genetic epilepsy models in elucidating early mechanisms leading to an epileptogenic state. The remarkable efficacy of FEN in this DS model demonstrates the utility of zebrafish in uncovering potential disease-modifying activity of drug leads.

ACKNOWLEDGMENTS

The authors thank A. C. Sulen Tavara, R. Steen Kolve, D. Wroblewski, N. T. Mathabela, S. Mishra, and H. Tandberg for excellent fish care; and Uni Research Bergen, D. Fischer, and J. Jacoby for their generosity and support in

15281167, 2020, 3, Downloaded from https://onlinelibrary.wiley.com/doi/10.1111/epi.16456 by Ku Leuven, Wiley Online Library on [31/10/2022]. See the Terms and Conditions (https://onlinelibrary.wiley.com/terms-and-conditions) on Wiley Online Library for rules of use; OA articles are governed by the applicable Creative Commons License

enabling the creation of the *scn1lab* zebrafish line. C.V.E. is funded by a Center for Molecular Medicine Norway startup grant. K.G. received funding from the European Union's Horizon 2020 research and innovation program under the Marie Skłodowska-Curie Action (grant agreement No. 798703-GEMZ-H2020-MSCA-IF-2017). A.S. is funded by the National Research Fund of Luxembourg through C14/BM/7975668/CaSCAD and INTER/DFG/17/11583046 MechEPI (Mechanisms of Epileptogenesis).

CONFLICT OF INTEREST

None of the authors has any conflict of interest to disclose. We confirm that we have read the Journal's position on issues involved in ethical publication and affirm that this report is consistent with those guidelines.

DATA AVAILABILITY STATEMENT

Supporting data are available as supplementary materials or, upon request, from the corresponding author. scRNA-Seq data will be made available online through Gene Expression Omnibus.

ORCID

Camila V. Esguerra https://orcid.org/0000-0002-2271-8094

REFERENCES

1. Dravet C. The core Dravet syndrome phenotype. Epilepsia. 2011;52(2):3–9.
2. Claes L, Del-Favero J, Ceulemans B, et al. De novo mutations in the sodium-channel gene SCN1A cause severe myoclonic epilepsy of infancy. Am J Hum Genet. 2001;68:1327–32.
3. Steel D, Symonds JD, Zuberi SM, Brunklaus A. Dravet syndrome and its mimics: beyond SCN1A. Epilepsia. 2017;58:1807–16.
4. Marini C, Scheffer IE, Nabbout R, et al. The genetics of Dravet syndrome. Epilepsia. 2011;52(2):24–9.
5. Harkin LA, McMahon JM, Iona X, et al. The spectrum of SCN1A-related infantile epileptic encephalopathies. Brain J Neurol. 2007;130:843–52.
6. Ogiwara I, Miyamoto H, Morita N, et al. Nav1.1 localizes to axons of parvalbumin-positive inhibitory interneurons: a circuit basis for epileptic seizures in mice carrying an Scn1a gene mutation. J Neurosci. 2007;27:5903–14.
7. Rutecki PA, Grossman RG, Armstrong D, Irish-Loewen S. Electrophysiological connections between the hippocampus and entorhinal cortex in patients with complex partial seizures. J Neurosurg. 1989;70:667–75.
8. Chabardès S, Kahane P, Minotti L, et al. The temporopolar cortex plays a pivotal role in temporal lobe seizures. Brain J Neurol. 2005;128:1818–31.
9. Kelsom C, Lu W. Development and specification of GABAergic cortical interneurons. Cell Biosci. 2013;3:19.
10. Pelkey KA, Chittajallu R, Craig MT, Tricoire L, Wester JC, McBain CJ. Hippocampal GABAergic inhibitory interneurons. Physiol Rev. 2017;97:1619–47.
11. Tsai MS, Lee ML, Chang CY, et al. Functional and structural deficits of the dentate gyrus network coincide with emerging spontaneous seizures in an Scn1a mutant Dravet syndrome model during development. Neurobiol Dis. 2015;77:35–48.
12. Ceulemans B, Boel M, Leyssens K, et al. Successful use of fenfluramine as an add-on treatment for Dravet syndrome. Epilepsia. 2012;53:1131–9.
13. Polster T. Individualized treatment approaches: fenfluramine, a novel antiepileptic medication for the treatment of seizures in Dravet syndrome. Epilepsy Behav. 2019;91:99–102.
14. Martin P, Maurice T, Gammaitoni A, et al. Fenfluramine has in vivo activity as a positive allosteric modulator of sigma-1 receptors. Poster presented at: American Epilepsy Society Annual Meeting; December 1-5, 2017; Washington, DC.
15. Lagae L, Sullivan J, Cross H, et al.ZX008 (fenfluramine) in Dravet syndrome: results of a phase 3, randomized, double-blind, placebo-controlled trial. Poster presented at: American Epilepsy Society Annual Meeting; December 1-5, 2017; Washington, DC.
16. Zhang Y, Kecskés A, Copmans D, et al. Pharmacological characterization of an antisense knockdown zebrafish model of Dravet syndrome: inhibition of epileptic seizures by the serotonin agonist fenfluramine. PLoS One. 2015;10:e0125898.
17. Connolly HM, Crary JL, McGoon MD, et al. Valvular heart disease associated with fenfluramine-phentermine. N Engl J Med. 1997;337:581–8.
18. Knupp KG, Wirrell EC. Treatment strategies for Dravet syndrome. CNS Drugs. 2018;32:335–50.
19. Baraban SC, Taylor MR, Castro PA, Baier H. Pentylenetetrazole induced changes in zebrafish behavior, neural activity and c-fos expression. Neuroscience. 2005;131:759–68.
20. Afrikanova T, Serruys AS, Buenafe OE, et al. Validation of the zebrafish pentylenetetrazol seizure model: locomotor versus electrographic responses to antiepileptic drugs. PLoS One. 2013;8:e54166.
21. Balciunas D, Wangensteen KJ, Wilber A, et al. Harnessing a high cargo-capacity transposon for genetic applications in vertebrates. PLoS Genet. 2006;2:e169.
22. Zijlmans M, Jiruska P, Zelmann R, Leijten FS, Jefferys JG, Gotman J. High-frequency oscillations as a new biomarker in epilepsy. Ann Neurol. 2012;71:169–78.
23. Livak KJ, Schmittgen TD. Analysis of relative gene expression data using real-time quantitative PCR and the 2(-Delta Delta C(T)) method. Methods. 2001;25:402–8.
24. Macosko EZ, Basu A, Satija R, et al. Highly parallel genome-wide expression profiling of individual cells using nanoliter droplets. Cell. 2015;161(5):1202–14.
25. Ferreira TA, Blackman AV, Oyrer J, et al. Neuronal morphometry directly from bitmap images. Nat Methods. 2014;11:982–4.
26. Ristanović D, Milosević NT, Stulić V. Application of modified Sholl analysis to neuronal dendritic arborization of the cat spinal cord. J Neurosci Methods. 2006;158:212–8.
27. Baraban SC, Dinday MT, Hortopan GA. Drug screening in Scn1a zebrafish mutant identifies clemizole as a potential Dravet syndrome treatment. Nat Commun. 2015;4.
28. Dinday MT, Baraban SC. Large-scale phenotype-based antiepileptic drug screening in a zebrafish model of Dravet syndrome. eNeuro. 2015;2:8–9.
29. McNally JM, McCarley RW. Gamma band oscillations: a key to understanding schizophrenia symptoms and neural circuit abnormalities. Curr Opin Psychiatry. 2016;29:202–10.

15281167, 2020, 3, Downloaded from https://onlinelibrary.wiley.com/doi/10.1111/epi.16456 by Ku Leuven, Wiley Online Library on [31/10/2022]. See the Terms and Conditions (https://onlinelibrary.wiley.com/terms-and-conditions) on Wiley Online Library for rules of use; OA articles are governed by the applicable Creative Commons License

30. Mistry AM, Thompson CH, Miller AR, Vanoye CG, George AL Jr, Kearney JA. Strain- and age-dependent hippocampal neuron sodium currents correlate with epilepsy severity in Dravet syndrome mice. Neurobiol Dis. 2014;65:1–11.
31. Hedrich UB, Liautard C, Kirschenbaum D, et al. Impaired action potential initiation in GABAergic interneurons causes hyperexcitable networks in an epileptic mouse model carrying a human Na(V)1.1 mutation. J Neurosci. 2014;34:14874–89.
32. De Lanerolle NC, Kim JH, Robbins RJ, Spencer DD. Hippocampal interneuron loss and plasticity in human temporal lobe epilepsy. Brain Res. 1989;49:387–95.
33. Robbins RJ, Brines ML, Kim JH, et al. A selective loss of somatostatin in the hippocampus of patients with temporal lobe epilepsy. Ann Neurol. 1991;29:325–32.
34. Sundstrom LE, Brana C, Gatherer M, Mepham J, Rougier A. Somatostatin- and neuropeptide Y-synthesizing neurones in the fascia dentata of humans with temporal lobe epilepsy. Brain J Neurol. 2001;124:688–97.
35. Mathern GW, Babb TL, Pretorius JK, Leite JP. Reactive synaptogenesis and neuron densities for neuropeptide Y, somatostatin, and glutamate decarboxylase immunoreactivity in the epileptogenic human fascia dentata. J Neurosci. 1995;15:3990–4004.
36. Swartz BE, Houser CR, Tomiyasu U, et al. Hippocampal cell loss in posttraumatic human epilepsy. Epilepsia. 2006;47:1373–82.
37. Houser CR. Do structural changes in GABA neurons give rise to the epileptic state? Adv Exp Med Biol. 2014;813:151–60.
38. Cobos I, Calcagnotto ME, Vilaythong AJ, et al. Mice lacking Dlx1 show subtype-specific loss of interneurons, reduced inhibition and epilepsy. Nat Neurosci. 2005;8:1059–68.
39. Yu FH, Mantegazza M, Westenbroek RE, et al. Reduced sodium current in GABAergic interneurons in a mouse model of severe myoclonic epilepsy in infancy. Nat Neurosci. 2006;9:1142–9.
40. Schoonheim PJ, Arrenberg AB, Del Bene F, Baier H. Optogenetic localization and genetic perturbation of saccade-generating neurons in zebrafish. J Neurosci. 2010;30:7111–20.
41. Silenieks LB, Carroll NK, Van Niekerk A, et al. Evaluation of selective 5-HT2C agonists in acute seizure models. ACS Chem Neurosci. 2019;10(7):3284–95.
42. Paizanis E, Kelaï S, Renoir T, Hamon M, Lanfumey L. Life-long hippocampal neurogenesis: environmental, pharmacological and neurochemical modulations. Neurochem Res. 2007;32:1762–71.
43. Daubert EA, Heffron DS, Mandell JW, Condron BG. Serotonergic dystrophy induced by excess serotonin. Mol Cell Neurosci. 2010;44:297–306.
44. Reid CA, Leaw B, Richards KL, et al. Reduced dendritic arborization and hyperexcitability of pyramidal neurons in a Scn1b-based model of Dravet syndrome. Brain. 2014;137:1701–15.
45. Sofroniew MV, Vinters HV. Astrocytes: biology and pathology. Acta Neuropathol. 2010;119:7–35.
46. Hawkins NA, Calhoun JD, Huffman AM, Kearney JA. Gene expression profiling in a mouse model of Dravet syndrome. Exp Neurol. 2019;311:247–56.
47. Favero M, Sotuyo NP, Lopez E, Kearney JA, Goldberg EM. A transient developmental window of fast-spiking interneuron dysfunction in a mouse model of Dravet syndrome. J Neurosci. 2018;38:7912–27.
48. Hawkins NA, Zachwieja NJ, Miller AR, Anderson LL, Kearney JA. Fine mapping of a Dravet syndrome modifier locus on mouse chromosome 5 and candidate gene analysis by RNA-Seq. PLoS Genet. 2016;12(10):e1006398.
49. Kang SK, Hawkins NA, Kearney JA. C57BL/6J and C57BL/6N substrains differentially influence phenotype severity in the Scn1a+/− mouse model of Dravet syndrome. Epilepsia Open. 2019;4:164–9.

SUPPORTING INFORMATION

Additional supporting information may be found online in the Supporting Information section.

How to cite this article: Tiraboschi E, Martina S, van der Ent W, et al. New insights into the early mechanisms of epileptogenesis in a zebrafish model of Dravet syndrome. *Epilepsia*. 2020;61:549–560. https://doi.org/10.1111/epi.16456

15281167, 2020, 3, Downloaded from https://onlinelibrary.wiley.com/doi/10.1111/epi.16456 by Ku Leuven, Wiley Online Library on [31/10/2022]. See the Terms and Conditions (https://onlinelibrary.wiley.com/terms-and-conditions) on Wiley Online Library for rules of use; OA articles are governed by the applicable Creative Commons License